THE JOURNAL OF PHYSICAL CHEMISTRY Letters

Cite This: J. Phys. Chem. Lett. 2019, 10, 5830−5835

Letter

pubs.acs.org/JPCL

Edge Phonon Excitations in a Chiral Self-Assembled Supramolecular Nanoribbon

José D. Cojal González,[†] Juan Li,[‡,∥] Meike Stöhr,[§] Milan Kivala,[⊥] Carlos-Andres Palma,*[,†,‡] and Jürgen P. Rabe[†]

[†]Department of Physics & IRIS Adlershof, Humboldt-Universität zu Berlin, Newtonstr. 15, 12489 Berlin, Germany

[‡]Institute of Physics, Chinese Academy of Sciences, 10090 Beijing, P.R. China

[∥]Advanced Research Institute of Multidisciplinary Science, Beijing Institute of Technology, 100081 Beijing, P.R. China

[§]Zernike Institute for Advanced Materials, University of Groningen, Nijenborgh 4, 9747 AG Groningen, The Netherlands

[⊥]Organisch-Chemisches Institut & Centre for Advanced Materials, Ruprecht-Karls-Universität Heidelberg, Im Neuenheimer Feld 270 & 225, 69120 Heidelberg, Germany

Supporting Information

ABSTRACT: By design, coupled mechanical oscillators offer a playground for the study of crystalline topology and related properties. Particularly, non-centrosymmetric, supramolecular nanocrystals feature a complex phonon spectrum where edge modes may evolve. Here we show, employing classical atomistic calculations, that the edges of a chiral supramolecular nanoribbon can host defined edge phonon states. We suggest that the topology of several edge modes in the phonon spectrum is nontrivial and thermally insulated from bulk states. By means of molecular dynamics, we excite a supramolecular bond to launch a directional excitation along the edge without considerable bulk or back-propagation. Our results suggest that supramolecular monolayers can be employed to engineer phonon states that are robust against backscattering, toward supramolecular thermal waveguides, diodes, and logics.

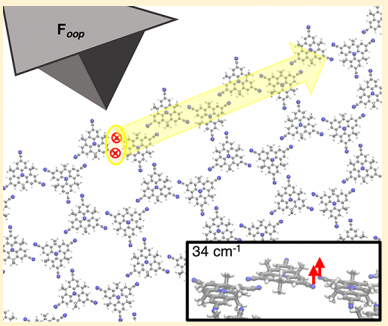

Two-dimensional (2D) molecular architectures at interfaces[1−3] have been the focus of proof-of-concept semiconducting,[4] sensitizing,[5] dipolar doping,[6] and nanopatterning[7] applications, to mention a few. Nanoscopic functional concepts have also been proposed, such as single-molecule transistor arrays,[8] memory arrays,[9] and thermal encoders.[10] Thus far, these concepts are adaptations of well-established technological strategies, offering moderate advantages over alternative 2D materials. The recent topological classification of solids promises to expand the scope of material engineering[11−13] alongside molecules at interfaces.[14] Among these, phononic materials replicate topologies encountered in Fermionic[15−17] single-particle Hamiltonians, albeit under dissipative conditions.[18,19] Because of their topological or mechanical isolation from the crystalline bulk, domain boundaries within such phonon materials lay the foundation for unidirectional phononic waveguiding[20−23] and logics.[24] Recently, these principles have been extended to two-dimensional (2D) crystals,[25] offering the prospect of engineering and realizing atomistic phonon devices with supramolecular architectures.

Archetypical "edge states" formed at domain walls are found in one-dimensional (1D) crystalline polyacetylene models such as the Su−Schrieffer−Heeger (SSH) model.[15,26] Modifying the supercell size and boundary of the model, as illustrated by a change in the resonance structure (Figure 1a), forces an edge state in the electronic structure characterized by a topological invariant[27,28] (Figure 1a). Another effective design strategy to engineer an edge state is to prepare a boundary along a (bipartite) honeycomb lattice[17,27,29] (Figure 1b). Nanoribbons are thus a common route for the preparation and engineering of phononic *dissipative* topological crystalline insulators (TCIs),[18,30] in analogy to their Fermionic counterparts.[31−33] In addition, non-centrosymmetric hexagonal lattices have been shown to host topologies beyond common TCIs, featuring nongapped band crossings such as Weyl points,[34,35] which are suggested to occur because of encounters between longitudinal and transverse phonon bands.[36] For most rigid and macroscopic isostatic materials, however, phonon properties are not straightforwardly engineered.[29] Because phononic states depend on nonbonded interactions, (2D) supramolecular materials might provide a versatile platform for topological phononic engineering,[37] in a manner similar to dipolar molecules in optical lattices.[38,39]

Here we show that distinct edge modes are present in a 2D self-assembled supramolecular architecture (Figure 1c). We employ an atomistic molecular mechanics and dynamics approach, which allows us not only to predict the existence of independent transversal, longitudinal and hybrid edge modes, but also to excite them and provide mechanistic

Received: July 10, 2019
Accepted: September 11, 2019
Published: September 19, 2019

DOI: 10.1021/acs.jpclett.9b02001
J. Phys. Chem. Lett. 2019, 10, 5830−5835

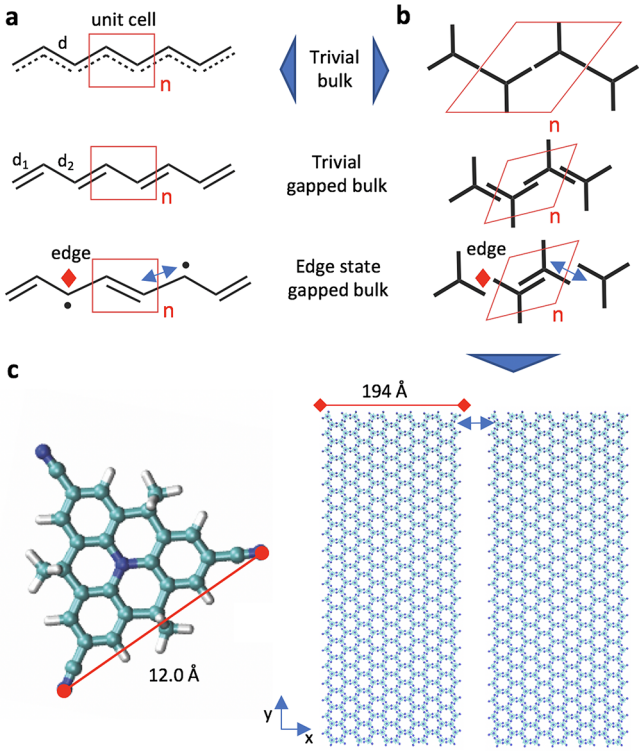

Figure 1. Edge states in supramolecular nanoribbons (SNR). (a) Modifying the structure's symmetry (d_1 and d_2) and boundary (blue arrow) in a polyacetylene model opens an electronic gap and induces an electronic edge state with a defined topology. (b) Assuming a similar Hamiltonean, a vibrational (phononic) gap and edge state can be induced in a chiral honeycomb lattice. (c) We have shown that a tricyano-substituted bridged triarylamine derivative **1** can self-assemble into a chiral 2D supramolecular layer with zigzag edges (cf. Figure S1).

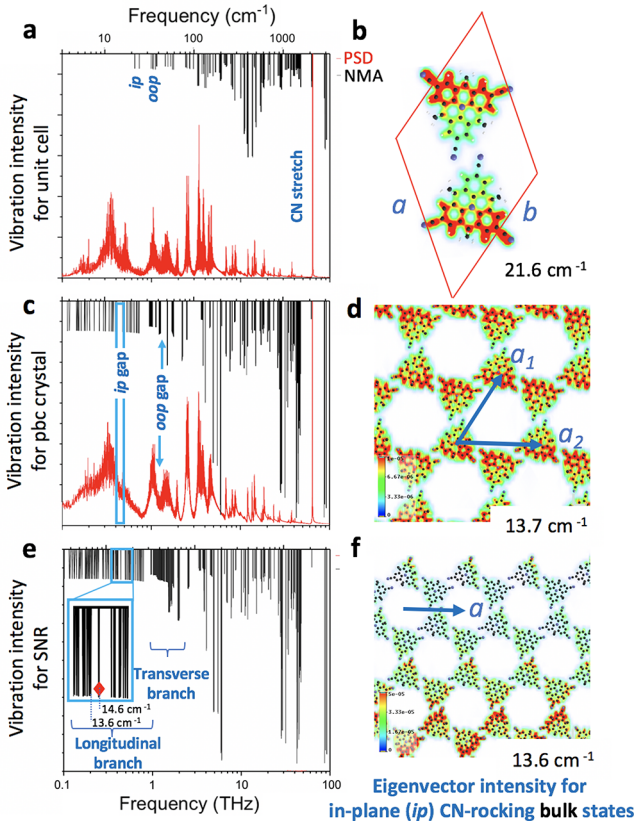

Figure 2. From molecular vibrations to phonons. Harmonic (NMA, black) and anharmonic (PSD, red) vibrational spectra (a, c, and e) and eigenvector intensity maps (b, d, and f) for (a and b) a unit cell of **1**, (c and d) a 5800-atom periodic boundary condition (pbc) crystal and (e and f) a supramolecular nanoribbon (SNR). The SNR is generated by lifting the periodicity of the pbc crystal in the x direction, following the design in Figure 1c. Typical bulk states derived from a librational in-plane (ip) rocking mode are mapped in panels b, d, and f ($a = a_1 = 23.62$ Å).

insights into their directional propagation. The employed tools are widespread and atom-centered, which encourage fast calculations along eigenmodes and the prototyping of supramolecular materials with desired characteristics. Our work places supramolecular architectures in the map of phononic materials with potential topological properties and within the context of supramolecular mechanical engineering for the development of (organic) thermal logic[10] and telecommunication.

Organic and supramolecular crystals are often characterized by unit cells of hundreds of atoms, making phonon spectrum interpretation challenging. For supramolecular 2D crystals, the study of low-energy librational modes in single molecules is a valid departure point for the understanding of phonons in such complex matter.[40] Therefore, we investigate the low-energy vibrations in a weak hydrogen-bonded dimeric $a = b = 23.62$ Å elementary unit cell self-assembled system (Figure 2a,b), which we have shown yields chiral zigzag-edged architectures (Figure S1). The chiral monolayer is composed of tricyano-substituted, bridged triarylamine **1** (4,4,8,8,12,12-hexamethyl-4*H*,8*H*,12*H*-benzo[1,9]quinolizino[3,4,5,6,7-*defg*]acridine-2,6,10-tricarbonitrile, Figure S2).[41,42] We investigate the harmonic and anharmonic vibrations and phonons in such molecular architectures by means of harmonic normal-mode analysis (NMA), velocity autocorrelation function (VACF), and molecular dynamics (MD) simulations.[43,44]

The NMA of the unit cell places the lowest energy mode at 21.6 cm^{-1} (Figure 2a,b), which corresponds to a CN frustrated rotation mode or in-plane (ip) "rocking" of the unit cell. A neighboring mode at 30.4 cm^{-1} is identified as an out-of-plane (oop) CN mode (Figure S3). Mostly discrete modes evolve from the unit cell's NMA, as the normal modes are constrained to the number of degrees of freedom in the bimolecular elementary unit cell. Because of this, Born−Huang dynamical matrix methods are usually employed for phonon spectra calculations, yet they pose convergence challenges for increasingly large numbers of different atoms (e.g., a 11600-atom nanoribbon). Instead, the phonon density of states for a periodic unit can be efficiently extracted via the power spectral density (PSD) from the VACF in molecular dynamic calculations[45] (Figure 2a, red) or NMA calculations at the infinite atom limit. We thus construct a 5800-atom crystal and correspondingly 17400 modes (its relaxed structure retains the unit cell $a_1 = a_2 = 23.62$ Å). The intensity profile of the low-energy NMA spectrum (Figure 2c, black) now closely resembles the PSD at 200 K (Figure 2c, red) and 50 K (Figure S4, red), discussed in detail below. One intense PSD branch is centered around 10 cm^{-1} and is assigned to CN ip modes: The mapping in Figure 2d identifies a 13.7 cm^{-1} mode as a delocalized mode, correlating to the unit cells' ip "rocking" mode along the high-symmetry a_2 [100] direction. A

DOI: 10.1021/acs.jpclett.9b02001
J. Phys. Chem. Lett. 2019, 10, 5830−5835

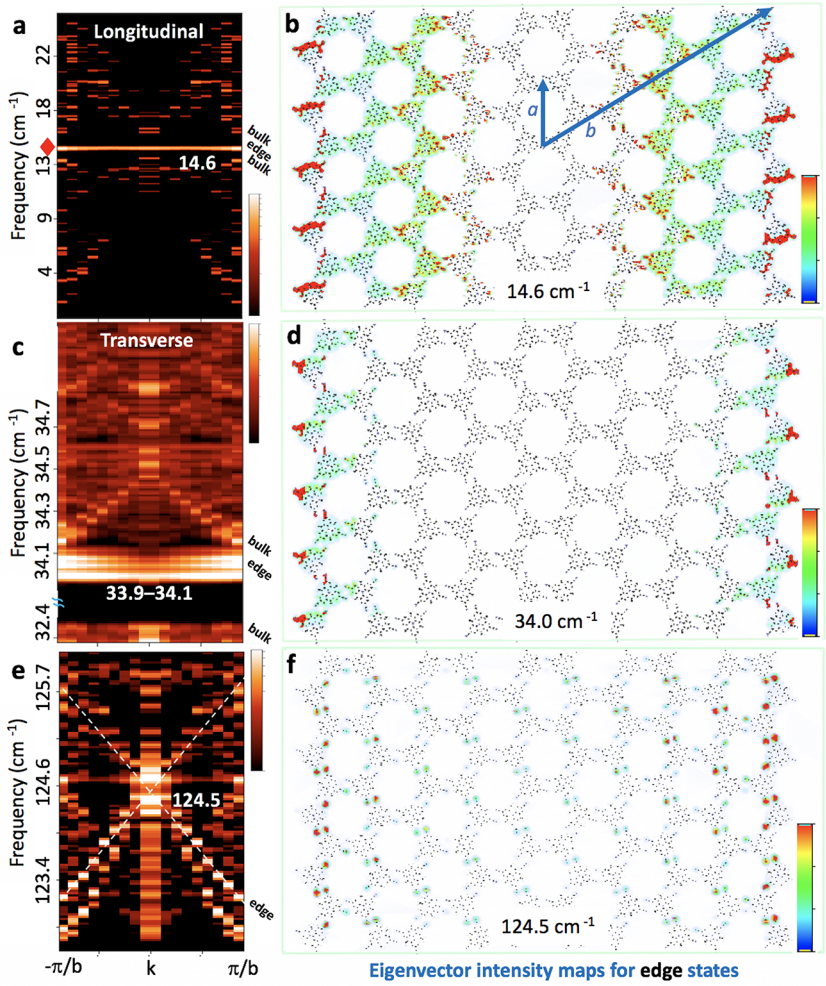

Figure 3. Edge phonons in a supramolecular nanoribbon. Band structure (a, c, and e) and eigenvector maps (b, d, and f) along *b* for (a and b) the first longitudinal edge phonon (in the 0.1−0.9 THz branch region), (c and d) the first transversal edge phonon (in the 1−2 THz region), and (e and f) a transversal phonon (in the 2−4 THz region). Eigenvector intensity color scale (b and d) 5×10^{-4} to 0 and (f) 1×10^{-4} to 0 a = 23. 62 Å.

neighboring 15.9 cm^{-1} mode displays a "bending" mode, albeit in the a_1 direction. The gap between them corresponds to a valley in the 200 K PSD density of states (DOS). Another intense PSD branch is centered around 40 cm^{-1} and depicts several valleys roughly corresponding to gaps in the NMA spectrum. The gaps are named after the most intense modes of their corresponding PSD branches, centered at [13.7, 15.9] cm^{-1} (a 0.27 meV gap) for the ip gap and at [43.0, 50.0] cm^{-1} (a 0.86 meV gap) for the widest oop gap, and are characterized by a strong temperature dependence. For the PSD spectra at 50 K, peaks in the ip and oop branches and gaps are dramatically suppressed (Figure S4b, red), and their valleys broaden accordingly. Intense low-energy peaks retain their shape and energy at 50 K, e.g. the bulk 33 cm^{-1} (Figure S3) and the 64 cm^{-1} N−C oop umbrella mode (cf. the Supporting Information animation), indicating selective temperature effects. It is worth noting that the most intense signal in the PSD for all studied systems is the CN stretch, which amounts to 2085.5 cm^{-1} (at 50 and 200 K) versus 2085.0 cm^{-1} (NMA) and 2200 cm^{-1} (from infrared spectroscopy measurements at 298 K in the solid state[41,42]).

Next, an edge along the zigzag directions for the 5800-atom crystal is induced by removing the periodicity in the *x*-direction, as shown in Figure 1c. This operation affords a 194 Å-wide supramolecular nanoribbon with a unit cell vector identical to the periodic crystal vector of a = 23.62 Å, albeit with a contraction of intermolecular distances by 3% (0.8 Å) in the remaining high-symmetry directions. The NMA spectrum in Figure 2e shows that several modes move to the low-energy region, highlighting the two ip and oop band regions. The ip gap further expands to [13.6, 16.4] cm^{-1} (0.33 meV) while most of the oop gaps close. The bottom (top) band's 13.6 cm^{-1} (16.4 cm^{-1}) mode of the nanoribbon (Figure 2f) follows the point group symmetry of the crystal's ip mode with two main differences. The eigenvector's highest intensity follows direction a_2 and vanishes toward the edge. Moreover, a new state appears in the middle of the ip gap at 14.6 cm^{-1} (red diamond, Figure 2e).

Dispersion data along b (direction $[K, -K]$) from NMA eigenvector mapping (Figure 3a,b) depict the ip intragap edge state within a longitudinal bulk phonon branch. The branch is identified as longitudinal by inspecting the vibrational modes and plotting the eigenvector's ip and oop components (Figure S5). The 14.6 cm^{-1} edge state is 4-fold degenerate with an obvious edge signature, as shown by the merged map in Figure 3b. The edge state eigenvector intensity decays by 5 orders of magnitude into the bulk (Figure S6) and suggests the possibility of thermal guiding along the edges at the excitation

DOI: 10.1021/acs.jpclett.9b02001
J. Phys. Chem. Lett. 2019, 10, 5830−5835

wavelength. Yet calculation along the periodic crystallographic direction [*K*, *M*] reveals the state as a flat-band with negligible group velocity $\partial\omega\,\partial k^{-1} = 0$, which is in principle (see MD excitations below) unfavorable for phonon waveguiding purposes. We thus turn to the exploration of the phonon gaps in the next spectral branch, where transverse modes appear. The lowest energy, recognizable edge states in the branch are found at [33.9, 34.1] cm^{-1} comprising ten modes (Figure 3c,d). Eight states at 33.9 cm^{-1} (4.2 meV) decay with an amplitude attenuation of 8 orders of magnitude into the bulk (Figure S7). This edge phonon has a finite group velocity along the periodic ribbon direction, yet it does not sit in the middle of this oop gap: It connects to the bottom of a bulk phonon band sitting only 0.2 cm^{-1} higher, at 34.2 cm^{-1}, making its selective excitation challenging by isotropic stimuli. Nevertheless, a selective excitation of the edge mode by a point probe (see below) or polarized excitation is plausible (because of markedly different eigenvector symmetry of the nearby bulk modes, Figure S8).

The NMA makes it possible to depict edge eigenvectors without inversion symmetry (Figure S9a). A nonzero Berry phase or Zak phase[27] from a corresponding well-defined band is topologically protected, hinting toward possibilities in thermal waveguiding.[39] Because current atom-centered methods feature a limited k-space resolution (e.g., only few atoms in a 11600-atom supercell ribbon contribute to specific bands), we expect future work to unambiguously identify potentially competing band crossings and elucidate topological invariants under anharmonic, finite temperature, and dissipative conditions.

It is of interest to investigate higher-energy (3−5 THz) nongapped phonon density regions. At 124.6 cm^{-1}, we find a crossing of two linear transversal bands (Figure 3e). An edge state at 124.5 cm^{-1} is encountered, which derives from CN in-plane bending modes (Figure 3f). Unlike the previous edge mode at 34 cm^{-1}, where both ip and oop transversal components are present at the edges, mostly the ip component of this edge state plays a role. Here, one CN bond per molecule (a "lone" CN in Figure 3f) contributes to the edge mode intensity (Figure S10). These observations are expected to play a key role in the design of dispersion relations with particular energies. Though further development of high-resolution and efficient analytical methods suitable for molecules with a large number of atoms is required, our method unambiguously reveals the atomistic origin of phonon longitudinal and transversal edge bands.

To explore the excitation profile of the nanoribbon's edge, a single edge supramolecular bond is excited with a transversal force of 50 pN at the phonon edge band of 34 cm^{-1} (4.2 meV). Despite a limited bandwidth, the 34 cm^{-1} mode is highly localized along the edge (cf. Figure 3d), which translates to thermal insulation of the bulk upon excitation. The excitation is applied by means of a force oscillation routine at the corresponding excitation periods of 0.98 ps (48 K thermal equivalent) during Langevin molecular dynamic simulations at the lower temperature of 30 K. Mode excitation under these conditions is possible by, for instance, employing a local probe (tip) suitable for scanning (inelastic) tunneling microscopy or atomic force microscopy at cryogenic temperatures. The excitation along the edge is tracked by kinetic energy propagation. It reveals collective excitations along the edge (Figure 4b) and no perturbation into the bulk (Figure 4c), corroborating the insulating character of the bulk.

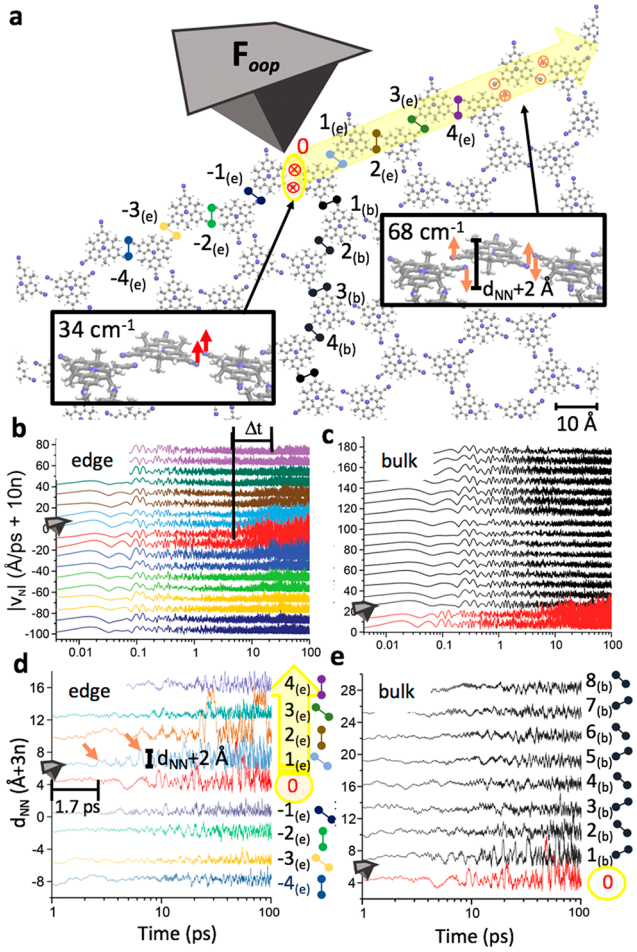

Figure 4. Guided excitation of an edge mode. (a) Two nitrogen atoms in a single edge supramolecular dimer in the nanoribbon are excited by an oscillating oop force (F_{oop}, marked by a virtual atomic force microscope tip) during molecular dynamics at 30 K. (b and c) The kinetic energy for the nitrogen along the supramolecular edge (marked in colors) and the bulk (marked black) are extracted, demonstrating localized heating of the edge. (d and e) The distance between neighboring N atoms reveals that structural perturbations propagate unidirectionally (yellow highlight). The insets in (a) reveal the initial in-phase perturbation (red arrows) and out-of-phase propagation after 1.7 ps (orange arrows).

Although the group velocity along the edge was found to be negligible from band structure calculations, the calculated propagation velocity can be measured from Figure 4b (black vertical lines): After $\Delta t \approx 20$ ps, the velocity of a molecule at a distance of 47 Å increases, indicating a propagation of ∼0.2 nm ps^{-1}. To better understand the mechanism of propagation, the geometrical fluctuations of the CN−CN distances (d_{NN}) for adjacent molecules are extracted (Figure 4d). These provide information about the coherence of the CN vibrations during propagation. As discussed above, the 34 cm^{-1} mode implies a concomitant oop rocking of the CN supramolecular pairs along the edge (red arrows Figure 4a inset, and Figure S7).

After 1.7 ps, the CN pairs oscillate out-of-phase (as shown by "peaks" in the d_{NN} spectrum) effectively doubling the propagation frequency to 68 cm^{-1}(orange arrows, Figure 4a inset). This frequency is absent from the NMA band structure (Figures 2e and S11) and might indicate a damped oscillator origin.[46] The decoherence of the 34 cm^{-1} shows a directional

DOI: 10.1021/acs.jpclett.9b02001
J. Phys. Chem. Lett. 2019, 10, 5830−5835

effect and provokes disturbances up to d_{NN} > 10 Å along one adjacent unit cell (CN no. $2_{(e)}$ in brown, Figure 4a,d), while the bulk and opposite edge direction remain unperturbed. The robustness of this noncoherent excitation against back-propagation is particular to the supercell of the nanoribbon, where the CN···H bonds are shorter every other molecule by 0.04 Å and straighter by 19°, effectively promoting an alternating "weak" and "strong" supramolecular bond at low temperatures which recalls the SSH model in Figure 1a. Intuitively, an excitation at the "weaker" supramolecular bond near the bulk axis (Figure 4a inset) will act as a mechanical lever along the strongly bonded dimer and propagation will favorably occur anisotropically. To substantiate this observation, we excite an adjacent "strong" CN···H bond and correspondingly corroborate isotropic propagation of the excitation (Figure S12). This behavior is reproduced in Langevin simulations employing different initial velocity assignments and friction coefficients. We expect the choice of thermostats and damping functions to spark interest in the chaotic dynamics of topological (molecular) materials at finite temperatures.

We have demonstrated that two-dimensional supramolecular materials can exhibit rich phononic characteristics. In the particular case of non-centrosymmetric honeycomb supramolecular assemblies which have been previously reported, localized longitudinal and transverse edge modes, insulated from the bulk, are present in normal-mode analysis. These phonon states can be measured by employing scanning probe microscopy at inert interfaces and low temperatures, aided by previously reported methodologies.[40] Within our classical dynamics model, we show that the excitation of the edge propagation modes is mechanically protected against back-propagation, towards thermal waveguiding and thermal diodes. We expect further (quantum) design of supramolecular nanoribbons and architectures to aid in the prediction and realization of atomistic thermal devices.

■ ASSOCIATED CONTENT

Supporting Information

The Supporting Information is available free of charge on the ACS Publications website at DOI: 10.1021/acs.jpclett.9b02001.

Methods and Figures S1−S13 (PDF)

Simulation files, structural files, animations, and parameters (ZIP)

■ AUTHOR INFORMATION

Corresponding Author

*E-mail: palma@iphy.ac.cn.

ORCID

Meike Stöhr: 0000-0002-1478-6118

Carlos-Andres Palma: 0000-0001-5576-8496

Jürgen P. Rabe: 0000-0003-0847-6663

Notes

The authors declare no competing financial interest.

■ ACKNOWLEDGMENTS

We gratefully acknowledge financial support from the Alexander von Humboldt Foundation (C.-A.P.), the Deutsche Forschungsgemeinschaft (DFG) SFB 765 (J.D.C.G. and J.P.R.), SFB 953 (M.K.), Project No. 401247651-KI1662/3-1; from The Netherlands Organisation for Scientific Research (NWO), VIDI-grant No. 700.10.424, VENI-grant No. 722.012.010; and from the Foundation for Fundamental Research on Matter (FOM), part of the NWO (M.S.). C.-A.P. is grateful to Chunyin Qiu, Hongming Weng, and Xi Dai for preliminary discussions.

■ REFERENCES

(1) Rabe, J. P.; Buchholz, S. Commensurability and Mobility in Two-Dimensional Molecular Patterns on Graphite. *Science* **1991**, *253*, 424−427.

(2) Jung, T. A.; Schlittler, R. R.; Gimzewski, J. K. Conformational Identification of Individual Adsorbed Molecules with the STM. *Nature* **1997**, *386*, 696−698.

(3) Barth, J. V.; Costantini, G.; Kern, K. Engineering Atomic and Molecular Nanostructures at Surfaces. *Nature* **2005**, *437*, 671−679.

(4) He, D.; Zhang, Y.; Wu, Q.; Xu, R.; Nan, H.; Liu, J.; Yao, J.; Wang, Z.; Yuan, S.; Li, Y.; Shi, Y.; Wang, J.; Ni, Z.; He, L.; Miao, F.; Song, F.; Xu, H.; Watanabe, K.; Taniguchi, T.; Xu, J.-B.; Wang, X. Two-Dimensional Quasi-Freestanding Molecular Crystals for High-Performance Organic Field-Effect Transistors. *Nat. Commun.* **2014**, *5*, 5162.

(5) Wieghold, S.; Li, J.; Simon, P.; Krause, M.; Avlasevich, Y.; Li, C.; Garrido, J. A.; Heiz, U.; Samorì, P.; Müllen, K.; Esch, F.; Barth, J. V.; Palma, C.-A. Photoresponse of Supramolecular Self-Assembled Networks on Graphene−Diamond Interfaces. *Nat. Commun.* **2016**, *7*, 10700.

(6) Gobbi, M.; Bonacchi, S.; Lian, J. X.; Vercouter, A.; Bertolazzi, S.; Zyska, B.; Timpel, M.; Tatti, R.; Olivier, Y.; Hecht, S.; Nardi, M. V.; Beljonne, D.; Orgiu, E.; Samorì, P. Collective Molecular Switching in Hybrid Superlattices for Light-Modulated Two-Dimensional Electronics. *Nat. Commun.* **2018**, *9*, 2661.

(7) Madueno, R.; Raisanen, M. T.; Silien, C.; Buck, M. Functionalizing Hydrogen-Bonded Surface Networks with Self-Assembled Monolayers. *Nature* **2008**, *454*, 618−621.

(8) Jäckel, F.; Watson, M. D.; Müllen, K.; Rabe, J. P. Prototypical Single-Molecule Chemical-Field-Effect Transistor with Nanometer-Sized Gates. *Phys. Rev. Lett.* **2004**, *92*, 188303.

(9) Liljeroth, P.; Repp, J.; Meyer, G. Current-Induced Hydrogen Tautomerization and Conductance Switching of Naphthalocyanine Molecules. *Science* **2007**, *317*, 1203−1206.

(10) Palma, C.-A.; Björk, J.; Klappenberger, F.; Arras, E.; Kühne, D.; Stafström, S.; Barth, J. V. Visualization and Thermodynamic Encoding of Single-Molecule Partition Function Projections. *Nat. Commun.* **2015**, *6*, 6210.

(11) Haldane, F. D. M. Model for a Quantum Hall Effect without Landau Levels: Condensed-Matter Realization of the "Parity Anomaly". *Phys. Rev. Lett.* **1988**, *61*, 2015−2018.

(12) Hasan, M. Z.; Kane, C. L. Colloquium: Topological Insulators. *Rev. Mod. Phys.* **2010**, *82*, 3045.

(13) Zhang, T.; Jiang, Y.; Song, Z.; Huang, H.; He, Y.; Fang, Z.; Weng, H.; Fang, C. Catalogue of Topological Electronic Materials. *Nature* **2019**, *566*, 475−479.

(14) Yan, L.; Liljeroth, P. Engineered Electronic States in Atomically Precise Nanostructures: Artificial Lattices and Graphene Nanoribbons. arXiv preprint, arXiv:1905.03328; 2019.

(15) Rice, M.; Mele, E. Elementary Excitations of a Linearly Conjugated Diatomic Polymer. *Phys. Rev. Lett.* **1982**, *49*, 1455.

(16) Cheon, S.; Kim, T.-H.; Lee, S.-H.; Yeom, H. W. Chiral Solitons in a Coupled Double Peierls Chain. *Science* **2015**, *350*, 182−185.

(17) Yves, S.; Fleury, R.; Berthelot, T.; Fink, M.; Lemoult, F.; Lerosey, G. Crystalline Metamaterials for Topological Properties at Subwavelength Scales. *Nat. Commun.* **2017**, *8*, 16023.

(18) Esaki, K.; Sato, M.; Hasebe, K.; Kohmoto, M. Edge States and Topological Phases in Non-Hermitian Systems. *Phys. Rev. B: Condens. Matter Mater. Phys.* **2011**, *84*, 205128.

DOI: 10.1021/acs.jpclett.9b02001
J. Phys. Chem. Lett. 2019, 10, 5830−5835

(19) Lieu, S. Topological Phases in the Non-Hermitian Su-Schrieffer-Heeger Model. *Phys. Rev. B: Condens. Matter Mater. Phys.* **2018**, *97*, 045106.
(20) Huber, S. D. Topological Mechanics. *Nat. Phys.* **2016**, *12*, 621.
(21) Lu, J.; Qiu, C.; Ye, L.; Fan, X.; Ke, M.; Zhang, F.; Liu, Z. Observation of Topological Valley Transport of Sound in Sonic Crystals. *Nat. Phys.* **2017**, *13*, 369.
(22) Xia, B.-Z.; Liu, T.-T.; Huang, G.-L.; Dai, H.-Q.; Jiao, J.-R.; Zang, X.-G.; Yu, D.-J.; Zheng, S.-J.; Liu, J. Topological Phononic Insulator with Robust Pseudospin-Dependent Transport. *Phys. Rev. B: Condens. Matter Mater. Phys.* **2017**, *96*, 094106.
(23) Fan, H.; Xia, B.; Tong, L.; Zheng, S.; Yu, D. Elastic Higher-Order Topological Insulator with Topologically Protected Corner States. *Phys. Rev. Lett.* **2019**, *122*, 204301.
(24) Pirie, H.; Sadhuka, S.; Wang, J.; Hoffman, J. E. Topological Phononic Logic. arXiv preprint, arXiv:1809.09187; 2018.
(25) Jin, Y.; Wang, R.; Xu, H. Recipe for Dirac Phonon States with a Quantized Valley Berry Phase in Two-Dimensional Hexagonal Lattices. *Nano Lett.* **2018**, *18*, 7755−7760.
(26) Su, W. P.; Schrieffer, J.; Heeger, A. J. Solitons in Polyacetylene. *Phys. Rev. Lett.* **1979**, *42*, 1698.
(27) Zak, J. Berry's Phase for Energy Bands in Solids. *Phys. Rev. Lett.* **1989**, *62*, 2747.
(28) Delplace, P.; Ullmo, D.; Montambaux, G. Zak Phase and the Existence of Edge states in Graphene. *Phys. Rev. B: Condens. Matter Mater. Phys.* **2011**, *84*, 195452.
(29) Kane, C.; Lubensky, T. Topological Boundary Modes in Isostatic Lattices. *Nat. Phys.* **2014**, *10*, 39.
(30) Pal, R. K.; Vila, J.; Leamy, M.; Ruzzene, M. Amplitude-Dependent Topological Edge States in Nonlinear Phononic Lattices. *Phys. Rev. E: Stat. Phys., Plasmas, Fluids, Relat. Interdiscip. Top.* **2018**, *97*, 032209.
(31) Palma, C.-A.; Awasthi, M.; Hernandez, Y.; Feng, X.; Müllen, K.; Niehaus, T. A.; Barth, J. V. Sub-Nanometer Width Armchair Graphene Nanoribbon Energy Gap Atlas. *J. Phys. Chem. Lett.* **2015**, *6*, 3228−3235.
(32) Cao, T.; Zhao, F.; Louie, S. G. Topological Phases in Graphene Nanoribbons: Junction States, Spin Centers, and Quantum Spin Chains. *Phys. Rev. Lett.* **2017**, *119*, 076401.
(33) Gröning, O.; Wang, S.; Yao, X.; Pignedoli, C. A.; Barin, G. B.; Daniels, C.; Cupo, A.; Meunier, V.; Feng, X.; Narita, A.; et al. Engineering of Robust Topological Quantum Phases in Graphene Nanoribbons. *Nature* **2018**, *560*, 209−213.
(34) Lu, L.; Wang, Z.; Ye, D.; Ran, L.; Fu, L.; Joannopoulos, J. D.; Soljačić, M. Experimental Observation of Weyl Points. *Science* **2015**, *349*, 622−624.
(35) Lv, B. Q.; Weng, H. M.; Fu, B. B.; Wang, X. P.; Miao, H.; Ma, J.; Richard, P.; Huang, X. C.; Zhao, L. X.; Chen, G. F.; et al. Experimental Discovery of Weyl Semimetal TaAs. *Phys. Rev. X* **2015**, *5*, 031013.
(36) Zhang, T.; Song, Z.; Alexandradinata, A.; Weng, H.; Fang, C.; Lu, L.; Fang, Z. Double-Weyl Phonons in Transition-Metal Monosilicides. *Phys. Rev. Lett.* **2018**, *120*, 016401.
(37) Prodan, E.; Prodan, C. Topological Phonon Modes and Their Role in Dynamic Instability of Microtubules. *Phys. Rev. Lett.* **2009**, *103*, 248101.
(38) Yao, N. Y.; Gorshkov, A. V.; Laumann, C. R.; Läuchli, A. M.; Ye, J.; Lukin, M. D. Realizing Fractional Chern Insulators in Dipolar Spin Systems. *Phys. Rev. Lett.* **2013**, *110*, 185302.
(39) Shi, T.; Cirac, J. I. Topological Phenomena in Trapped-Ion Systems. *Phys. Rev. A: At., Mol., Opt. Phys.* **2013**, *87*, 013606.
(40) Palma, C.-A.; Joshi, S.; Hoh, T.; Ecija, D.; Barth, J. V.; Auwärter, W. Two-Level Spatial Modulation of Vibronic Conductance in Conjugated Oligophenylenes on Boron Nitride. *Nano Lett.* **2015**, *15*, 2242−2248.
(41) Gottardi, S.; Müller, K.; Moreno-López, J. C.; Yildirim, H.; Meinhardt, U.; Kivala, M.; Kara, A.; Stöhr, M. Cyano-Functionalized Triarylamines on Au (111): Competing Intermolecular Versus Molecule/Substrate Interactions. *Adv. Mater. Interfaces* **2014**, *1*, 1300025.
(42) Müller, K.; Moreno-López, J. C.; Gottardi, S.; Meinhardt, U.; Yildirim, H.; Kara, A.; Kivala, M.; Stöhr, M. Cyano-Functionalized Triarylamines on Coinage Metal Surfaces: Interplay of Intermolecular and Molecule−Substrate Interactions. *Chem. - Eur. J.* **2016**, *22*, 581−589.
(43) Brooks, B. R.; Brooks, C. L., III; Mackerell, A. D., Jr; Nilsson, L.; Petrella, R. J.; Roux, B.; Won, Y.; Archontis, G.; Bartels, C.; Boresch, S.; et al. Charmm: The Biomolecular Simulation Program. *J. Comput. Chem.* **2009**, *30*, 1545−1614.
(44) Warshel, A.; Lifson, S. Consistent Force Field Calculations. II. Crystal Structures, Sublimation Energies, Molecular and Lattice Vibrations, Molecular Conformations, and Enthalpies of Alkanes. *J. Chem. Phys.* **1970**, *53*, 582−594.
(45) Koukaras, E. N.; Kalosakas, G.; Galiotis, C.; Papagelis, K. Phonon Properties of Graphene Derived from Molecular Dynamics Simulations. *Sci. Rep.* **2015**, *5*, 12923.
(46) Deymier, P. A.; Runge, K.; Vasseur, J. Geometric Phase and Topology of Elastic Oscillations and Vibrations in Model Systems: Harmonic Oscillator and Superlattice. *AIP Adv.* **2016**, *6*, 121801.

DOI: 10.1021/acs.jpclett.9b02001
J. Phys. Chem. Lett. 2019, 10, 5830−5835